

# Asymmetric split ring resonators for optical sensing of organic materials

Basudev Lahiri<sup>1</sup>, Ali Z. Khokhar<sup>1</sup>, Richard M. De La Rue<sup>1</sup>, Scott G. McMeekin<sup>2</sup>  
and Nigel P. Johnson<sup>1\*</sup>

<sup>1</sup>Department of Electronics and Electrical Engineering, University of Glasgow, Glasgow, G12 8LT, UK

<sup>2</sup>School of Computing and Engineering, Glasgow Caledonian University, Glasgow, G4 0BA, UK

\*Corresponding author: [njohnson@elec.gla.ac.uk](mailto:njohnson@elec.gla.ac.uk)

**Abstract:** Asymmetric Split Ring Resonators are known to exhibit resonant modes where the optical electric field is strongest near the ends of the arms, thereby increasing the sensitivity of spectral techniques such as surface enhanced Raman scattering (SERS). By producing asymmetry in the structures, the two arms of the ring produce distinct plasmonic resonances related to their lengths – but are also affected by the presence of the other arm. This combination leads to a steepening of the slope of the reflection spectrum between the resonances that increases the sensitivity of the resonant behavior to the addition of different molecular species. We describe experimental results, supported by simulation, on the resonances of a series of circular split ring resonators with different gap and section lengths – at wavelengths in the mid-infra red regions of the spectrum - and their utilization for highly sensitive detection of organic compounds. We have used thin films of PMMA with different thicknesses, resulting in characteristic shifts from the original resonance. We also demonstrate matching of asymmetric split ring resonators to a molecular resonance of PMMA.

©2009 Optical Society of America

**OCIS codes:** (250.0250) Optoelectronics, (250.5403) Plasmonics, (240.6490) Spectroscopy, surface, (280.4788) Optical sensing and sensors.

---

## References and links

1. C. Debus and P. H. Bolivar, "Frequency selective surfaces for high sensitivity terahertz sensing," *Appl Phys Lett*, **91**, 184102-1 - 184102-3 (2007).
2. C. Debus and P. H. Bolivar, "Terahertz biosensors based on double split ring arrays," *Proc. SPIE*, **6987**, 6987(OU-1-8) (2008).
3. V. A. Fedotov, M. Rose, S. L. Prosvirnin, N. Papasimakis, and N. I. Zheludev, "Sharp Trapped-Mode Resonances in Planar Metamaterials with a Broken Structural Symmetry," *Phys Rev Lett*, **99**, 147401-1-4 (2007).
4. M. S. Rill, C. Plet, M. Thiel, I. Staude, G.V. Freymann, S. Linden, and M. Wegener, " Photonic metamaterials by direct laser writing and silver chemical vapour deposition," *Nature Materials* **7**, 543 - 546 (2008).
5. M. Brucherseifer, M. Nagel, P. H. Bolivar, H. Kurz, A. Bosserhoff, and R. Büttner, " Label-free probing of the binding state of DNA by time-domain terahertz sensing," *Appl. Phys. Lett.* **77**, 4049 -4051 (2000).
6. J. Aizpurua, T. Taubner, F. Javier Garcia de Abajo, M. Brehm, and R. Hillenbrand, " Substrate-enhanced infrared near-field spectroscopy," *Opt. Express* **16**, 1529-1545 (2008).
7. F. Neubrech, A. Pucci, T.W. Cornelius, S. Karim, A. Garcia-Etxarri, and J. Aizpurua, " Resonant Plasmonic and Vibrational Coupling in a Tailored Nanoantenna for Infrared Detection," *Phys Rev Lett.* **101**, 157403-1-4 (2008).
8. J. F. Federici, B. Schulkin, F. Huang, D. Gary, R. Barat, F. Oliveira, and D. Zimdars, "THz imaging and sensing for security applications - explosives, weapons and drugs," *Semicond. Sci. Technol.* **20**, S266-280 (2005).
9. M. Nagel and H. Kurz, "Corrugated waveguide based genomic biochip for marker-free THz read-out," *Int. J. Infrared Millim. Waves* **27**, 517-529 (2006).

10. H. Yoshida, Y. Ogawa, Y. Kawai, S. Hayashi, A. Hayashi, C. Otani, E. Kato, F. Miyamaru, and K. Kawase, "Terahertz sensing method for protein detection using a thin metallic mesh," *Appl. Phys. Lett.* **91**, 253901-1-3 (2007).
11. M. Nagel, P. Bolivar, and H Kurz., "Modular parallel-plate THz components for cost-efficient biosensing systems," *Semicond. Sci. Technol.* **20**, S281-S285 (2005).
12. E. M. Larsson, J. Alegret, M. Käll, and D. S. Sutherland, "Sensing Characteristics of NIR Localized Surface Plasmon Resonances in Gold Nanorings for Application as Ultrasensitive Biosensors," *Nano Lett.* **7**, 1256-1263 (2007).
13. D.H. Williams and I. Fleming, *Spectroscopic methods in Organic Chemistry* (McGraw Hill Publications, 2<sup>nd</sup> Edition 1973), Chap. 2.
14. A. Balamurugan, S. Kannan, V. Selvaraj, and S. Rajeswari, "Development and Spectral Characterization of Poly(Methyl Methacrylate)/Hydroxyapatite Composite for Biomedical Applications," *Trends Biomater. Artif. Organs*, **18** 41-45 (2004).

---

## 1. Introduction

Optical sensing of organic compounds has recently generated much interest, due to the wide range of applications that involve detection and characterization of organic materials. Using terahertz (THz) frequency electromagnetic waves, it is possible to sense the complex dielectric properties of a sample of material by detecting the resonant absorption or phonon resonance for molecular compounds [1-7]. For many applications, e.g. security, forensic analysis and immuno-sensing, sensitive detection of minute amounts of chemical and biochemical substances is required [8]. Various approaches are available, for example: microstrip wave guides [9], metallic meshes [10] and parallel plate microcavities [11]. High sensitivity terahertz biosensors typically have resonant structures in which the frequency response is modified by changes in their dielectric environment [1]. The resulting frequency shift depends on the characteristics of the dielectric modification - and hence can be used for its sensitive and accurate detection. The resonant frequencies of the structures scale inversely with size - with rings of ~12 mm diameter for frequencies around 8 GHz and ~ 100  $\mu\text{m}$  diameters for 1 THz. By increasing the resonant frequency into the infra-red spectral region, certain advantages are obtained. Firstly, a reduction in the overall size of the structure to ~1  $\mu\text{m}$  increases the intrinsic sensitivity to thin films or partial thin films deposited on the structure. Secondly, it is possible to tune the resonance to coincide with the spectral features of a selected organic functional group in the infra-red region of the spectrum - which may be useful for the detection of certain organic molecules. Here we report on a passive frequency-selective surface (FSS) based approach at infra-red wavelengths, using arrays of asymmetric Split Ring Resonator (A-SRRs) with a circular basic geometry. Our A-SRRs have a diameter of 1.2  $\mu\text{m}$ , with a strip width of 100 nm, and are fabricated in thin gold films on fused silica substrates. The characteristic resonances of such structures are in the mid-infrared (typically at wavelengths in the 3 - 6  $\mu\text{m}$  range). Split Ring Resonators (SRRs) have been shown to produce a high resonant electric field strength and modal intensity concentration near the ends of their arms [1-3]. The asymmetries between the two arms of the double SRR structures produce distinct plasmon resonances that are modified by the presence of the other arm, leading to a steep gradient of the reflection versus frequency curve between the resonances - and thereby increasing the sensitivity by comparison with similar but symmetric SRRs (S-SRRs), as has been described in references [1] and [2].

## 2. Fabrication and measurement

The patterns are generated on fused silica substrates using standard electron-beam lithography (EBL) processes, with the addition of an aluminum charge dissipation layer deposited over the bi-layer of PMMA resist. After development, the pattern is subjected to electron-beam deposition of 2 nm of titanium for adhesion, then 48 nm of gold, followed by lift-off. The patterns are written over an area of ~300 x 300  $\mu\text{m}$ . The reflection spectra of the fabricated structures have been measured at normal incidence with a Nicolet Continuum FTIR apparatus equipped with an Optical Microscope - using a 10 x magnification objective lens with an NA

of 0.25. The FTIR beam was polarized using a Continuum ZnSe IR polariser. An iris was used to restrict the incident light to a spot size area of nominally  $200\ \mu\text{m} \times 200\ \mu\text{m}$ . The reflectance measurements were taken with the incident light in one of two orthogonal polarizations - and were normalized, after each measurement, to the reflectivity of a gold mirror. Figure 1 shows a Scanning Electron Microscope (SEM) image of such a fabricated array of A-SRR patterns.

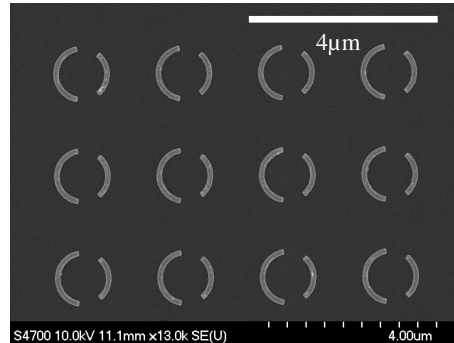


Fig. 1. SEM micrograph of A-SRRs with diameter  $1.2\ \mu\text{m}$  and  $100\ \text{nm}$  strip width.

### 3. Modeling

Modeling of the A-SRR structures was performed using the Fullwave FDTD simulation package from RSoft. A unit cell equal in dimensions to the period of the array of SRR structures, with periodic boundary conditions, was used to analyze the A-SRRs. The Drude model was used to describe the complex dielectric constant of the Au metal layer. The Ti adhesion layer was omitted from the simulation due to the increased computational time required to accommodate the required grid size. The resonant response of the A-SRR structures as a function of wavelength was modeled, together with the spatial electric field distribution at the various resonant wavelengths.

### 4. Asymmetric split ring resonators (A-SRRs)

The unit cell of a single A-SRR, as shown in Fig. 2, consists of two distinct and opposite single arcs separated by two identical narrow gaps. These two arcs (left-hand and right-hand) act as two separate resonators, with their individual resonance response depending on their respective length, as well as the angular gap between them. In our analysis we have varied the angular gap ( $\theta$ ) for the A-SRRs from  $\sim 10$  to  $50$  degrees, in steps of  $10$  degrees, by keeping the length of the left-hand arc constant and shortening the length of the right-hand arc. All the other parameters are identical.

Figure 3 depicts the resonant responses of arrays of symmetric and asymmetric SRR patterns obtained by measuring their corresponding reflectance spectra. In each case the measurements were made with light at normal incidence (i.e. the Z-direction) with the E-field maintained parallel to the Y direction. In the case of S-SRR1, the sizes of the left-hand and right-hand arcs are nominally identical (symmetric) - and their respective responses are superimposed, giving the overall resonance observed at  $4.11\ \mu\text{m}$ . This result has been confirmed using comparison with single arcs that have identical geometry. From A-SRR1 onwards, the right-hand arc is shortened progressively by varying  $\theta$ . As the angular gaps between the arcs are varied, the two separate resonances of the left-hand and right-hand arcs are modified by the presence of the other arc. In the case of A-SRR1, the asymmetry in length between the left and right-hand arc is still small - and a steep edge emerges at  $4.7\ \mu\text{m}$ , separating the resonance, at  $3.9\ \mu\text{m}$ , of the shorter (right-hand) arc from the resonance at  $4.9\ \mu\text{m}$  for the longer (left-hand) arc. (Between the two resonances, the reflection dip can be identified as a trapped mode [3], as discussed later). In the cases of A-SRR2 and A-SRR3, as the asymmetry between the lengths of the left-hand and right-hand arcs is varied further, the

individual resonances of the two arcs become more distinct - but, due to the proximity of the two arcs, the resonances observe are shifted with respect to those exhibited by single arcs alone.

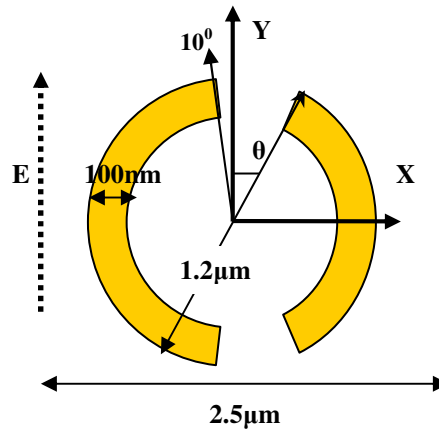


Fig. 2. A single unit cell with optimized dimensions, showing the orientation of the E-field parallel to the Y axis. Measurements have been carried out at normal incidence.

This result has been confirmed by simulations of separate arcs in which the individual peaks are closer together. A-SRR2 is marked by the steep edges that emerge in the reflection spectrum between the individual resonances of the left and right-hand arcs, with an increase in the quality factor from 4.7 for the symmetric case S-SRRs in Fig. 2(a) to 9.4 for the longer wavelength reflectance peak of A-SRR2 in Fig. 3(c). In the corresponding SRRs and A-SRRs with dimensions that lead to resonances in the microwave spectral region [3], at normal incidence the electric field of the linearly polarized plane-wave excitation can excite a circulating current that has the same direction in each arc – and therefore coupling into and out of such structures is inherently weak – and is zero, in principle, for the exactly symmetric case. In the case of asymmetry between the lengths of the two arcs, the scattered electromagnetic radiation produced by the circulating current configuration is weak but finite, reducing the coupling of the resonant mode to free space and reducing the radiation losses. This behavior leads to the so-called trapped mode identified by Fedetov et al [3]. When analyzing simulations of the transmission and reflection spectra, a substantial increase in the resonant absorption is observed at the minimum of the reflection dip corresponding to the trapped mode - and is consistent with energy being stored and dissipated in the coupled arcs.

For A-SRR3, there is a further shift in the resonance of the right-hand arc to shorter wavelengths, due to further reduction in its length. In the case of A-SRR4, the gap is further increased by additional shortening of the right-hand arc - so the impact of the loading of the non-resonant arc section on the resonance becomes small. Similar behavior is seen in the case of A-SRR5, where the angular gap is even further increased - resulting in the disappearance of the resonance produced by the shorter (right-hand) arc from the measured spectral range, as it increasingly moves towards shorter wavelengths. It can also be seen that, since the length of the left-hand arc is always kept constant, the resonance position of the longer (left hand) arc does not vary appreciably (moving only from 4.9  $\mu\text{m}$  to 4.6  $\mu\text{m}$ ). However, as the right-hand arc is shortened, it is found that the position of its resonance progressively moves towards shorter wavelengths (from 3.9  $\mu\text{m}$  to 2.5  $\mu\text{m}$ ), changing the spectra of the coupled resonance. It can therefore be inferred that variation of the angular gap between the two arcs not only increases the quality factor of the resonant peaks in the overall response, but also that it tunes the position of the resonances. The spike present at a wavelength of 4.2  $\mu\text{m}$  in all the experimental spectra indicates the presence of atmospheric carbon dioxide.

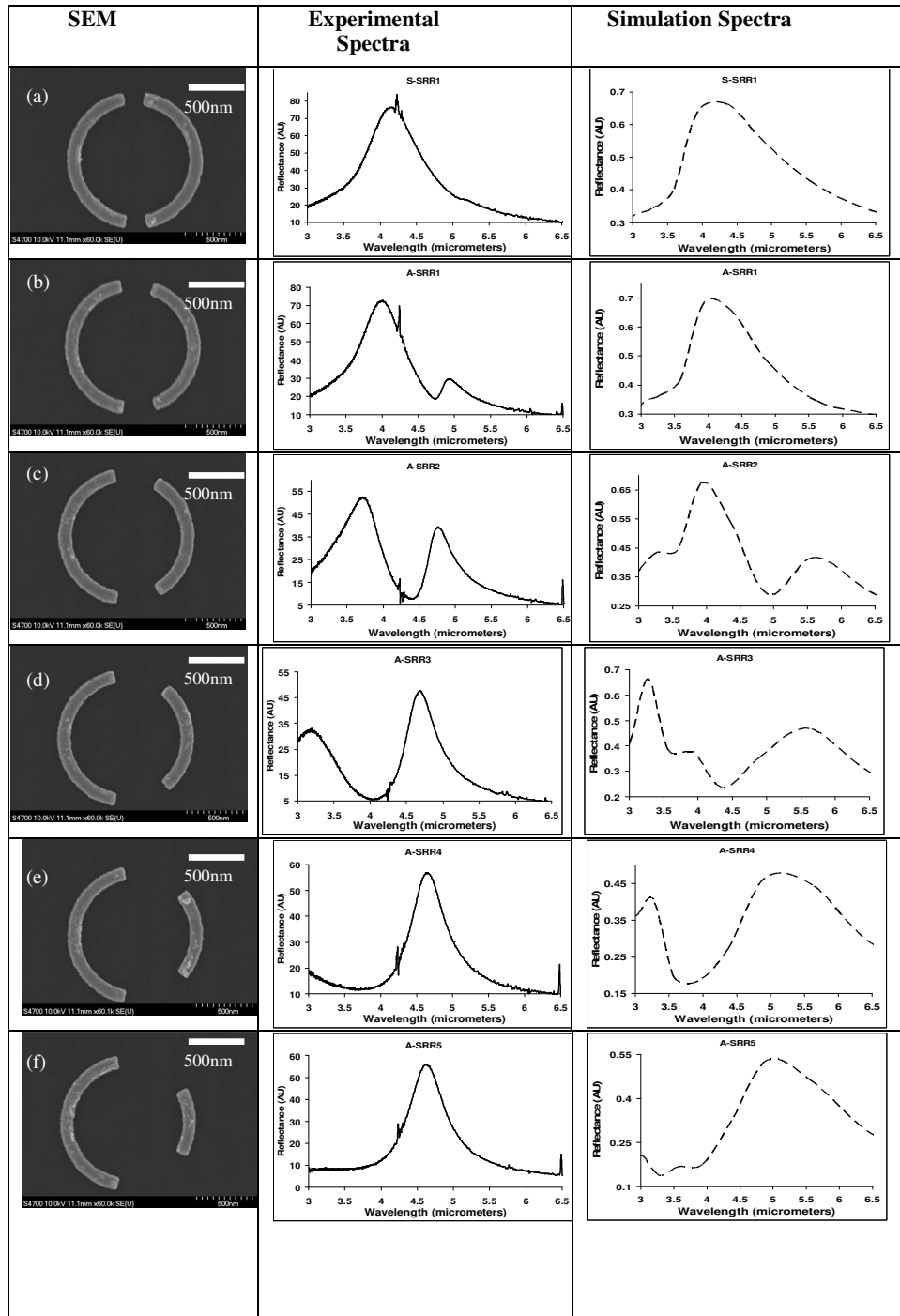


Fig. 3. Table showing the reflectance spectra of the different SRR patterns. The first column shows SEM images of the (a) S-SRR1 ( $\theta \sim 10^\circ$ ) (b) A-SRR1 ( $\theta \sim 15^\circ$ ) (c) A-SRR2 ( $\theta \sim 25^\circ$ ) (d) A-SRR3 ( $\theta \sim 35^\circ$ ) (e) A-SRR4 ( $\theta \sim 45^\circ$ ) (f) A-SRR5 ( $\theta \sim 55^\circ$ ) patterns. The second column of figures, with solid curves, shows the consequent experimental spectra – and the third column of figures, with dashed curves, show corresponding simulations.

Figure 4 shows the experimental spectrum for A-SRR2. This result is very much similar to that reported in [3], where a trapped mode resonant behavior was observed for structures with similar geometry at microwave frequencies – and also to the results for structures approximately a hundred times larger that have resonances in the low THz frequency region, as described in reference [2]. The Q-factor of the reflection dip of the trapped mode resonance is reduced from a figure of 20 in the microwave region, as reported in reference [3], down to an estimated value of 7, at the mid-infrared frequencies of the present work.

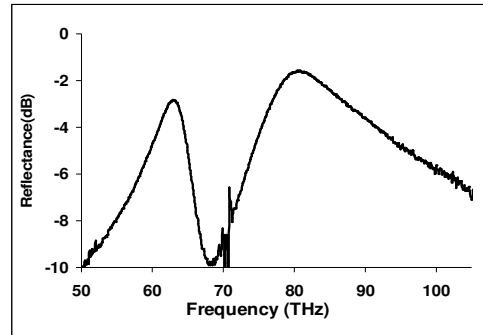


Fig. 4. The experimental reflection spectrum of A-SRR2 plotted as a function of frequency. The trough obtained at 68 THz is similar to the trapped mode observed in the microwave frequency range in reference [3].

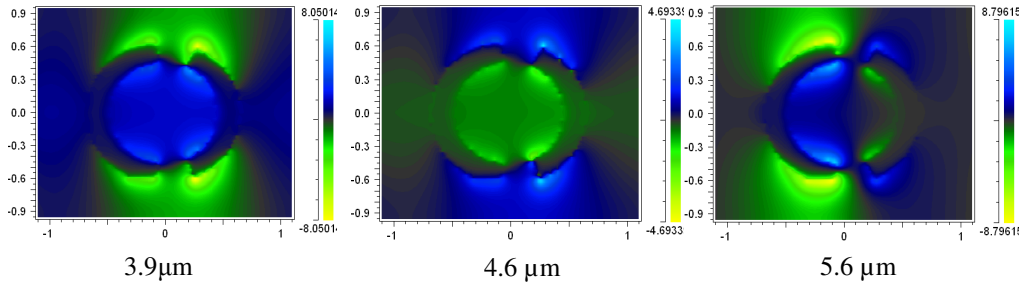


Fig. 5. Electric field strength in the Y direction at different wavelengths corresponding to the peaks and troughs in the simulation of Fig. 3(c).

The field plots in Fig. 5 show the concentration of the electric field distribution towards the ends of the arcs at a wavelength of 3.9  $\mu\text{m}$  for the smaller arc - and at a wavelength of 5.6  $\mu\text{m}$  for the larger arc. These wavelengths correspond to the respective reflection peaks. The central plot, at a wavelength of 4.6  $\mu\text{m}$ , corresponds to the reflectance dip of the trapped mode [3], for which the reflectance is sharply reduced and the field distribution in the two arcs is similar. Field enhancement factors associated with the edges of nanorings have been previously reported for the NIR and visible regions of the spectrum [12].

## 5. Detection of thin layers of PMMA

Many organic compounds contain molecular bonds that exhibit spectral resonances in the mid-infrared range (typically in the 3-5  $\mu\text{m}$  wavelength range) [12]. This property provides the main motivation, in our work, for tuning the resonant response of the A-SRRs to mid infrared wavelengths. In order to test the sensitivity of the A-SRRs, the fabricated structures were coated with thin films of poly-methyl-methacrylate (PMMA), a commonly used positive

electron-beam resist. The choice of PMMA in the present work was because of the accurate control of the thickness obtainable via control of the spin speed used when coating the sample. We have also observed a strong resonant feature at a wavelength of around  $5.8 \mu\text{m}$  due to absorption by the carbonyl bond of PMMA [13]. The use of PMMA as probe material for modifying the plasmonic behavior, has been described in reference [6]. Similar observation of enhanced infra-red detection of another organic molecule (ODT) is described in reference [7]. For our experiments, different concentrations of PMMA with molecular weights in the 80-100 k range and around 350 k, dissolved in o-xylene, were spun onto the A-SRR array at different speeds to give uniform thicknesses over the frequency-selective surface (FSS) pattern. The PMMA thickness was varied from 215 nm down to 30 nm, in order to test how effectively the A-SRRs were able to detect its presence. Fig. 6 shows the shift (experimental and simulation) in the overall resonant response of the A-SRRs obtained by loading the FSS pattern with 100 nm of PMMA. In the case of the S-SRR1 array, the overall shift due to the loading by the PMMA was less (typically around  $0.34 \mu\text{m}$  in the case of a 100 nm thick PMMA layer). In the case of A-SRR2, where the two distinct resonance peaks become clearly distinct, the shift observed in the position of the resonance was larger (typically around  $0.51 \mu\text{m}$  for a 100 nm thick PMMA layer).

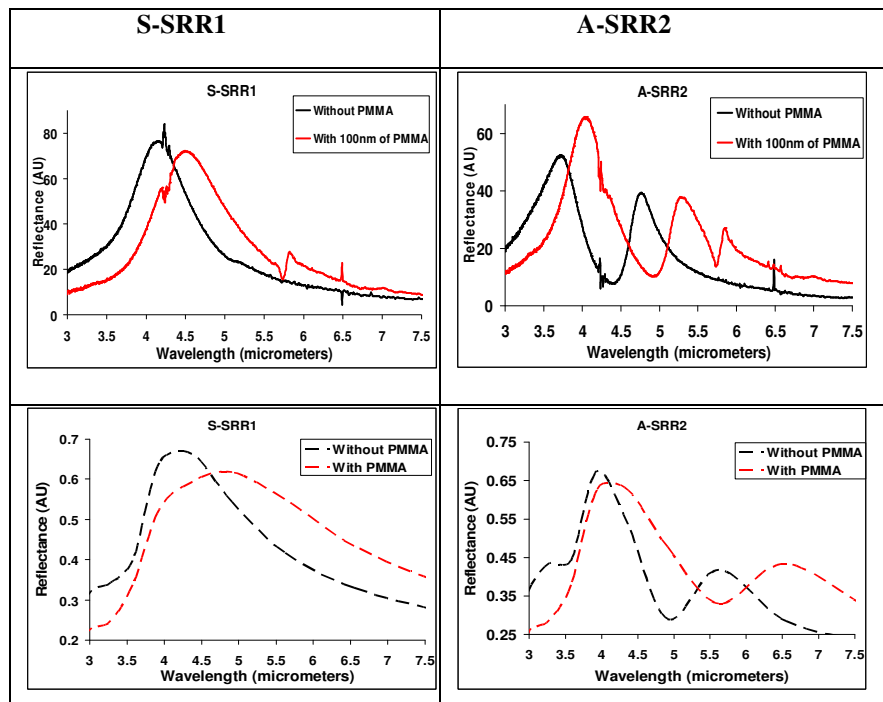


Fig. 6. Table depicting the shift in the position of the resonance produced by loading the A-SRR array with a 100 nm thick layer of PMMA. The first row with solid lines depicts the experimental results. The second row, with dashed lines in the figures, depicts the corresponding simulations. The black curves show the original resonance without PMMA and the red curves show the resonance with 100nm of PMMA deposited on top.

Simulations using a 100 nm dielectric layer of refractive index of  $\sim 1.49$  (Fig. 6) show a more significant broadening of the peaks compared to the experimental results. The model of the refractive index does not include the molecular absorption resonance or any wavelength dependence of the PMMA. Figure 7 shows the overall shift in the position of the resonances as a function of the thickness of the PMMA layer. Figure 7 shows that A-SRR2 can register

the presence of very thin layers of PMMA - as low as ~30 nm, which produces a shift in resonance of 120 nm. To act as an effective biosensor it will be necessary firstly to attach a vector to the rings that would act as a specific probe for a DNA strand. 30 nm corresponds to a polynucleotide length of around 100 base pair units.

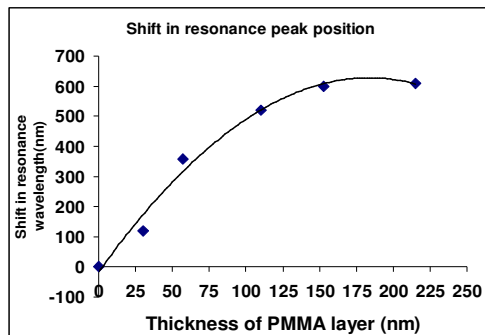


Fig. 7. Showing the shift in the position of the A-SRR2 longer wavelength resonance as a function of the thickness of the PMMA layer (solid line is a guide to the eye).

As the thickness of the PMMA increases, the shift in the peak position saturates, which can be attributed to the penetration of the propagating plasmonic mode beyond the PMMA layer becoming negligible. In order to detect the presence of small amounts of specific material - e.g. a particular DNA fragment [1-2], complementary receptors would need to be attached to the A-SSRs and, ideally, located near the ends of the arcs, where the electric field strength is greatest. By interpolation of the data in Fig. 7, it can be seen that a 5 nm uniform layer of PMMA would still produce a readily observable shift in the resonance peak position of around 25 nm – and, if the layer were localized near the ends of the arcs, the sensitivity should be significantly further increased.

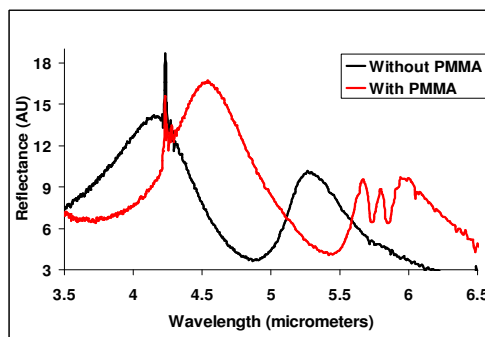


Fig. 8. The increase in sensitivity of PMMA obtained by matching the resonances. The black curve shows the original resonance without the PMMA - and the red curve shows the resonance with 100nm of PMMA deposited on top.

By changing the overall size of ASRR-2 from 1.2 to 1.35  $\mu\text{m}$  diameter it is possible to match the longer wavelength resonance of the arcs with the molecular resonance due to the carbonyl group of PMMA.

An example of the enhancement in the sensitivity is shown in Fig. 8 by the sharpened spectral feature with multiple peaks at around 5.8  $\mu\text{m}$ , as compared with the non-resonant behaviour at

the same wavelength in Fig 6. As the resonance of the A-SSR (by modifying the size) approaches that of the vibrational resonance the PMMA, the line shape is modified and results in an increase in the contrast of the PMMA signature.

## **6. Conclusions**

We have demonstrated similar behavior in asymmetric circular split ring resonators at size scales that are respectively two and four orders of magnitude smaller than those used in previous studies. While the Q-factor is reduced from 20 in the microwave range to 7 in the present work, the sensitivity to thin layers of organic material is significant, with a 120 nm resonance shift for 30 nm of PMMA. Two different sensing effects have been demonstrated: firstly the shift in the resonance due to the dielectric properties of the PMMA and secondly the change in line shape produced by matching the A-SSR resonances to a molecular resonance. Further enhancement is expected with localization of the organic material.

## **Acknowledgments**

The authors wish to acknowledge support from the European Commission through the Metamorphose NoE, ECONAM and COST action MP0702; and also the staff and facilities of the James Watt Nanofabrication Centre - and assistance from Anwesha Fernandes.